# A Machine learning-based approach for Picture Acquisition Timeslot Prediction using Defective Pixels

Farah Nafees Ahmed, Fouad Khelifi, Ashref Lawgaly and Ahmed Bouridane

Department of Computer and Information Sciences, Northumbria University, Newcastle upon Tyne, UK

**Abstract**

Estimating the acquisition time of digital photographs is a challenging task in temporal image forensics, but the application is highly demanded for establishing temporal order among individual pieces of evidence and deduce the causal relationship of events in a court case. The forensic investigator needs to identify the timeline of events and look for some patterns to gain a clear overview of activities associated with a crime. This paper aims to explore the presence of defective pixels over time for estimating the acquisition date of digital pictures. We propose a technique to predict the acquisition timeslots of digital pictures using a set of candidate defective pixels in non-overlapping image blocks. First, potential candidate defective pixels are determined through related pixel neighbourhood and two proposed features, called the local variation features to best fit in a machine learning model. The machine learning approach is used to model the temporal behaviour of camera sensor defects in each block using the scores obtained from individually trained pixel defect locations and fused in a majority voting method. Interestingly, timeslot estimation using individual blocks has been shown to be more accurate when virtual sub-classes corresponding to halved timeslots are first considered prior to the reconstruction step. Finally, the last stage of the system consists of the combination of block scores in a second majority voting operation to further enhance performance. Assessed on the NTIF image dataset, the proposed system has been shown to reach very promising results with an estimated accuracy between 88% and 93% and clear superiority over a related state-of-the-art system.

**Keywords**

Defective pixel detection, pixel classification, picture acquisition timeslot, temporal image forensics, defective pixel location, machine learning, digital evidence.

## 1. Introduction

In this new era of digital technology and with the usage of countless devices and applications, it is possible to keep track of pattern-of-life data points by the year, month, day, hour or even second. As more images and videos continue to flood the internet, the use of high-class digital technologies has changed the type of evidence that is now processed in forensic investigations. There may be many more audio, video and still images available of an actual crime than ever before. The forensic analyst can face challenges if there is any discrepancies or unreliability in digital evidences (Casey, 2020) . In forensic science, the primary purpose of forensic analysis is to do the complete investigation of the crime by reconstructing the events surrounding a crime using the available pieces of evidence (Casey et al., 2013) . These shreds of evidence are often used to sequence events, find locations, and establishing the time and duration of actions. Three common analysis techniques used in the forensic analysis are relational, functional and temporal analysis (Aquilina et al., 2008). Relational clues attempt to find out some relationship or interaction of object to the other object. Functional clues are used to find the way how it works or

how it functions. Temporal clues are based on temporal information or passage of time in which investigator tries to create a timeline of events and look for some patterns to gain a clear overview of events associated to a crime (Casey, 2009).

Meanwhile, data used in contemporary forensic investigations linked to crime events can be physical, digital or relational. The production of the timelines of events helps to resolve many forensic investigations, which are often now highly dependent on digital traces when physical traces are not present or tell only part of a story. Many such case studies are based on visualizing and constructing the sequences of events or activities captured by digital devices. The triple murder of Cody, Chad and Margaret Amato in Florida in January 2019 is a recent example of a temporal digital case which attracted much attention when forensic investigators handled the case by focusing on establishing the timeline of events captured by 35 different digital devices. Similarly, in 2015, a Connecticut man was arrested and charged with the killing of his wife after forensic staff produced a minute-by-minute timeline down of all of her movements during the relevant day which did not match his alibi. Nowadays, massive intensive forensic searches are based on the analysis of crime events to complete investigations involving murder, kidnap or rape. The temporal classification analysis of a specific device or set of devices helps the forensic analyst to frame the link of any crime incident or other event, and it mainly involves the collection of information within a particular timeframe so that the investigator can determine exactly when a particular crime or associated events happened (Ryser et al., 2020) . Temporal digital evidence can provide details of event sequences, activity levels and timing. Based on such evidences, the forensic analyst can answer questions about victims or suspects (‘who’), activities (‘what’), places (‘where’) and times (‘when’). Images and other visual recordings are important means to document at any instant in time the condition of specific subjects, which might include scenes related to a crime or accident, victims, suspects or any items of evidence. Such thorough and comprehensive photographic images of a scene, suspect or evidence from recordings made by a camera or any digital imaging technology can be helpful in identifying meaningful information which can lead to substantial or circumstantial evidence. If such images are presented in the court for investigation purposes, it is crucial that every possible measure should be taken to ensure the reliability and accuracy of picture dating. To correlate digital artifacts, the forensic analyst needs to process the correct ordering timeline of any relevant images to allow an understanding of the sequence of events. Helpful clues might be found in the file’s header (EXIF) when establishing a timeline as part of a digital forensic investigation. But, since this information could easily have been altered, it may be a significant challenge for the analyst to estimate the picture dating. The concept behind the temporal forensic analysis of an image is that the forensic investigator tries to estimate the acquisition time of any suspect images using some prior information or prior knowledge such as camera device or maybe set of images coming from the same devices taken at different time slots. As part of digital image forensics, it is essential to define additional information such as temporal parameters to estimate the time of acquisition of digital pictures taken by a camera and to know the conditions under which each picture was taken, such as exposure, date and time. For digitally born images, it is very easy to extract the date and thereby also easy to modify the settings for date and time. Consequently, there is no established technique that has been deployed in practical forensic investigations which allows the reliable extraction of temporal information from digital pictures. The increasing importance of temporal information needed in the forensic technique has created a need to develop the forensic techniques for temporal forensic image analysis.

In this paper, the dating of digital pictures is estimated by the temporal analysis of digital camera sensor imperfection using defective pixel locations. An algorithm is proposed that detects the image’s defective pixels behaviour over time to automate the picture dating — Section two elucidates the literature on detection of defective pixels and picture dating — the proposed system is presented in Section three. Section four discussed the experimental results and analysis. The conclusion is drawn in

Section five. The contribution of this paper can be summarized as follows. (i) To the best of our knowledge, this is the first work that combines defective pixel detection and machine learning for estimating the age of digital pictures. (ii) Two proposed features, called the first order and second order local variation features that can efficiently detect potential defective pixels for picture dating. (iii) A retraining-based approach using virtual sub-classes to estimate the timeslots in which digital images were taken more accurately. (iv) A multi-block based machine learning model that combines the predicted scores from multiples blocks to boost the performance of the system. The aforementioned contributions have been assessed and demonstrated through intensive experiments, accordingly.

## 2. Related Work

### 2.1. Detection of Defective Pixels

The digital image carries two types of fingerprint about the sensor. The Photo Response Non-Uniformity (PRNU) which is intrinsic that has been used in source camera identification and image authentication (Lukáš et al., 2006, Lawgaly et al., 2014, Al-Ani et al., 2015, Lawgaly and Khelifi, 2016, Gupta and Tiwari, 2018, Bernacki, 2020), and defective pixels which were used for image quality enhancement (El-Yamany, 2017, Dong et al., 2019). Like other microelectronic devices, digital imaging sensor develops defects over their lifetime and degrade with time gradually. Therefore, detection of defective pixels is still challenging.

In today's modern digital technologies, the increasing trend of using small pixel sizes and the higher sensitivity in the digital sensors enhanced the possibility of defective pixels (Chapman et al., 2011, Chapman et al., 2012, Igoe et al., 2018). The digital imager devices become more prone to pixel defects. Even they are in low quantity, they are very noticeable. (Chapman et al., 2018) highlighted that smart cell phones are more prone to pixel defects due to smaller size of pixels. They indicated that defective pixel accumulation is highly dependent on pixel size. In traditional digital cameras, the pixel size is about 4 to 7.5 $\mu m$ but in cell phones, the pixels are 1.34 $\mu m$ wide (Chapman et al., 2018) which drives more defective pixels. In the past, different studies explored the statistical nature of defective pixels as well as the source causing the anomalies for digital image sensors. Theuwissen (2007) indicated that defective pixels inside the camera sensor are caused due to imperfections in the silicon lattices. This damage is actually due to the impact of cosmic ray radiations that causes defective pixels, not material degradation. The defective pixels can be identified at the factory during the sensor manufacturing process. For instance, dark-frame calibration in factories is typically performed to identify the hot saturated pixels which are permanent hot pixels whereas light-field calibration is performed to detect the dead pixels which are less sensitive to illumination. However, the calibration process is expensive and complex at factory therefore, static defect maps during calibration process cannot be reliably used to represent the defective pixels over time in sensor. The number of research studies (Leung et al., 2007, Leung et al., 2008b, Leung et al., 2009, Chapman et al., 2012, Chapman et al., 2013) explored infield defects which vary across different imaging sensors and increased in number continuously over the sensors' lifetime. So such defects are likely to be caused by cosmic ray damage and hence any shielding or fabrication design changes cannot prevent them from developing over time (Chapman et al., 2019).

Defective pixels located in an image sensor often produce output differently from the neighbouring pixel outputs. Typically, pixel defects are categorized into different groups (Dudas et al., 2007, Chapman et al., 2013). They mainly are hot pixels (stuck high), dead pixels (stuck low) and abnormal-sensitivity pixels classified as partially stuck pixels. Hot pixels are those pixels

that produces output values much higher as compared to its neighbouring pixels. Stuck low pixels are those pixels whose values are much lower than from its adjacent pixels. They usually occur as black pixels. Partially stuck pixels are pixels whose values are different by a certain degree than its adjacent pixels (Chapman et al., 2005). The most prominent defective pixel types which occur in the sensor over its lifetime are stuck and hot pixels (Kauba and Uhl, 2016). The hot pixels are an independent illumination component and they increase linearly with exposure time. The detection rate of defective hot pixels gets enhanced when the ISO increases, especially when there is a low light condition (Leung et al., 2008a, Leung et al., 2009, Chapman et al., 2012, Chapman et al., 2013). Chapman et al. (2017) indicated that infield defects are always stuck hot pixels. Their analysis shows that when the size of the pixel shrinks, a large number of hot pixels produce at higher ISOs. They projected the hot pixel defect growth rate in terms of defect density (defects/year/mm$^2$) where the hot pixel densities grow through a power law. The power law of hot pixel is described with the inverse of the pixel size raised to the power of about 3 and the ISO parameter raised to the power of about 0.5. They developed special procedures to analyze the collected dark frame data where they found hot pixel defects growth rate become higher when the pixel size is reduced to 1 micron. Also, results shown in (Chapman et al., 2019) on cell phones indicate that defect density increases drastically when the pixel size falls below 2 microns. The quality of the digital images produced by digital sensors are mostly affected by dark current and hot pixels.

Kauba and Uhl (2016) detected the defective pixels in images by aligning the images pixel-wise based on PRNU sensor fingerprint to improve the biometric recognition. El-Yamany (2017) detect the defective pixels by exploiting Bayer sensors in the digital camera acquisition pipeline. They identified the defective pixel locations and updated the sensor defect map in order to produce high quality images. Dong et al. (2019) explore the digital image pipeline to detect the defective pixels by using multiple edge detection, detection channel and threshold segmentation. They built digital weld defect database to classify various defects through SVM classifier. Wang et al. (2019) proposed a blind pixel detection method based on visual characteristics to locate the dead pixels based on lower and higher than the other pixel values and obtain the pixel position information to fix the dead pixels. Forcina and Carbone (2020) formulated a statistical model called Gaussian mixture model to determine the effect of temperature and duration of exposure on dark current, hot pixels and thermal noise to analyze astronomical image data under darkness. Tchendjou and Simeu (2020) uses the pixel neighborhood analysis by taking only simple arithmetic operations on the neighborhood to detect the defective pixels. They estimated the distance between the under examination pixel and its surrounding pixels. They also computed mean, median, variance and other statistical dispersion parameters of the neighborhood pixels.

An interesting characteristic of defective pixels is that they accumulate over time and space on the sensor independently of each other. Thus, defective pixels once occurred in an imaging sensor, they continuously increased over time (Leung et al., 2009). They become a permanent part of the sensor which do not heal itself. Normally, it is expected for the digital camera sensor to show defects in a period of two months, approximately (Fridrich and Goljan, 2011). From this perspective, establishing temporal relationships between digital pictures taken by the same camera for dating purposes is theoretically possible when detecting the defective pixels on a temporal series of images which are spanned over a larger timespan. It's worth mentioning that the previously reviewed works on defective pixel detection were proposed for image quality enhancement unlike the current application which consists of using these potential pixels to estimate the acquisition date of images.

### 2.2. Picture Dating

With regards to picture dating, the previous studies estimated the picture dating particularly of those images which solely based on contents of images, for instance; finding the pattern of historical images (Palermo et al., 2012, Fernando et al., 2014), clothing styles or human appearances (Ginosar et al., 2015, Salem et al., 2016). Ginosar et al. (2015) and Salem et al. (2016) estimated the date of pictures through visual attributes by finding the pattern difference of human appearances, fashion and clothing styles. Palermo et al. (2012) proposed an approach to automatically predict the age of historical colour images in which they make a combination of various colour descriptors to model the historical colour photographs. They analysed the variations of colour distributions by using the colour statistics to classify the photographs while splitting the database into chronological time-order as well as taking consideration of capturing temporal discriminative information based on time. Fernando et al. (2014) further improved the Palermo et al. (2012) work by adding colour derivatives and angles. They noticed that extracting the colour distribution features are not efficient to discriminate between decades. Therefore, they proposed colour features which are device-dependent (such as colour-films) for dating historical colour images in which two colour descriptors such as RGB colour derivatives and colour angles attained for image dating purpose. Some of the research works such as Jae Lee et al. (2013) and Vittayakorn et al. (2017) looked for the visual style of objects to discover visual connection of images in space and time. Jae et al., (2013) evaluated and model stylistic differences across time and space by identifying the street and car object-type view images with different group of patches. The authors in Lee et al. (2015) used architecture styles as a cue to date pictures. Moreover, Martin et al. (2014) applied a binary classification algorithm to classify the image by deciding terms of 'older image' or 'newer image' when compared against a reference image. In He et al. (2016) research work, the age of historical documents is estimated by exploring contour and stroke fragments and applied CNN along with optical character recognition. Furthermore, Müller et al. (2017) predicted the acquisition of images, which were captured during the period from 1930 to 1999. Looking for the timestamp manipulation, some authors such as Kakar and Sudha (2012) and Li et al. (2017) worked on verifying the timestamp of images by estimating the sub azimuth angle with the help of shadow angles and sky appearance and then compared it according to the position of sun computed from the image metadata. In the research works of Padilha et al. (2021b), the authors verified the capturing date of images by looking the timestamp of images consistency with its scene content, geographic location and satellite imagery. Based on the appearance of the scene, the images from the real-world events are temporally sorted by estimating the image's temporal position within the duration of the event occurred (Padilha et al., 2021a) .

All of the above research works provide very impressive results however, the methods need the presence of particular visual elements in a scene and geographic location as a cues to reliably predict the time of images. Thus, previous studies estimate the dating of images based on the visual content of the images to identify the acquisition date of photographs. Moreover, many images were representing some historical events that directly linked the timeframes that the researchers were looking to envisage.

A very little research studies such as Fridrich and Goljan (2011) and Mao et al. (2009) have been devoted to the extraction of temporal localisation information from digital pictures. For temporal image forensics, the research study in Fridrich and Goljan (2011) uses natural images to identify the estimation of acquisition time of digital images. They used defective pixels for picture dating in the context of temporal forensic analysis. Taking advantage of defective pixels accumulation over time, Fridrich and Goljan (2011) exploited defective pixels to establish a temporal relationship between digital pictures taken by the same camera for dating purposes. They used maximum likelihood technique to estimate the defective pixel parameters and

detect the onset time to estimate the acquisition time of unknown digital pictures. They were unable to perform accurately between two consecutive defect onsets because the likelihood is constant. That is, the technique returns a constant acquisition time, which is the average time of the two onsets, for any given picture. So, the results were not so promising. The other research framework was presented by Mao et al. (2009) where the time-dependent camera parameters were assumed to be included in the PRNU. The results obtained through the correlation coefficients of PRNU estimates of different time-based image clusters showed the possibility to rank the clusters according to their acquisition date. The reported results have clearly shown that the correlation coefficient is not linearly dependent on the time span between the acquisition date of the picture under investigation and the date corresponding to the closest image cluster. Therefore, it would be theoretically incorrect to linearly map the correlation coefficient into a time span for dating purposes. Furthermore, the use of the correlation coefficient on the PRNU noise does not take the type of pixels into account and ignores their temporal evolution. That is, the correlation operation treats all the pixels equally without any prior knowledge on their temporal behaviour. Also, the dataset of images used in their studies are not in the sequential temporal order. Therefore, the researcher's work has not yet reached to accuracy results according to dating purposes.

## 3. Proposed Approach

The problem of estimating the acquisition date of digital pictures is formulated here as a classification problem where the system aims at predicting the right timeslot in which a query image was taken. Using a training and a validation subset, this work addresses the problem by training classifiers using pixel neighbourhood and two proposed local variation features to find best candidates of defective pixels for predicting the acquisition timeslots of digital pictures. It is based on the fact that the same pixel location for a series of images will be flagged as potentially defective if there is no change in the sensitivity of the pixel over time. With the help of multi-class classification, several training images taken at different times are grouped into a number of classes where each class corresponds to a timeslot, and the query image is assigned to one of them.

The high-level overview of the proposed system as presented in Figure 1 is divided into three stages in order to estimate the acquisition time of digital images. The first stage, as shown in Figure 1.1, aims at extracting a number of potential defective pixel locations from every image block and constructing reliable features using the pixel neighborhood in addition to the proposed local variation features. Such location-based features will be used to train classifiers where each classifier corresponds to a specific pixel location. Once the classifiers are trained for $M$ actual timeslots, the subset of validation images are used to rank the performance of such individual trained classifiers and consequently identify the $K$ best locations of potential pixel defects. This is to filter out the low-performance classifiers because they can negatively affect the overall performance if they are included at the final stage. In the second stage, as shown in Figure 1.2a, the system is retrained only for the best selected locations of pixel defects which show higher performance as explained earlier but for virtual sub-classes. Indeed, every actual timeslot is halved to create two virtual timeslots. This allows the system to get trained with a more challenging problem (i.e., more classes with shorter timeslots) so that when the scores get fused and reconstructed for the actual classes, performance can be boosted. In Figure 1.2b, a virtual timeslot is predicted for every individual block using the scores obtained from individually trained pixel defect locations. The predicted virtual timeslots are then considered in the reconstruction step to determine the predicted actual timeslot for a query image and fused in a majority voting method. Finally, Figure 1.3 represents the last stage of the system which consists of the combination of block-based prediction scores in a second majority voting operation to boost the performance.

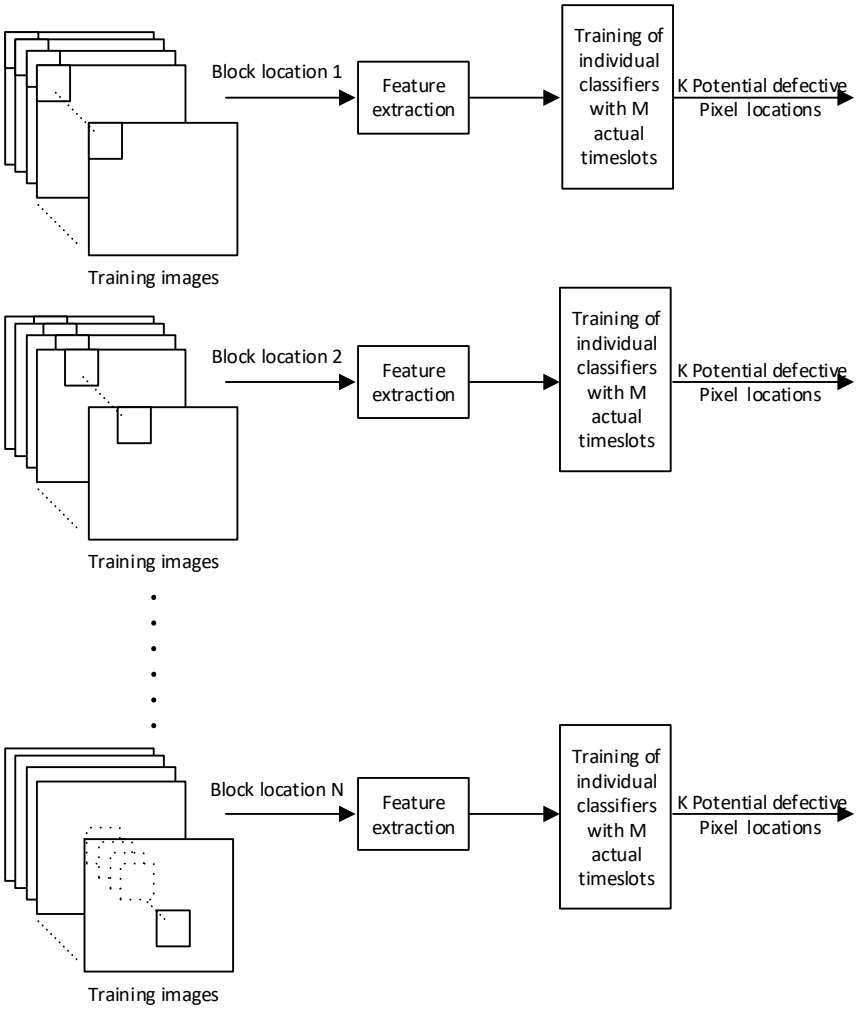


Fig 1.1. First Stage of the Proposed System

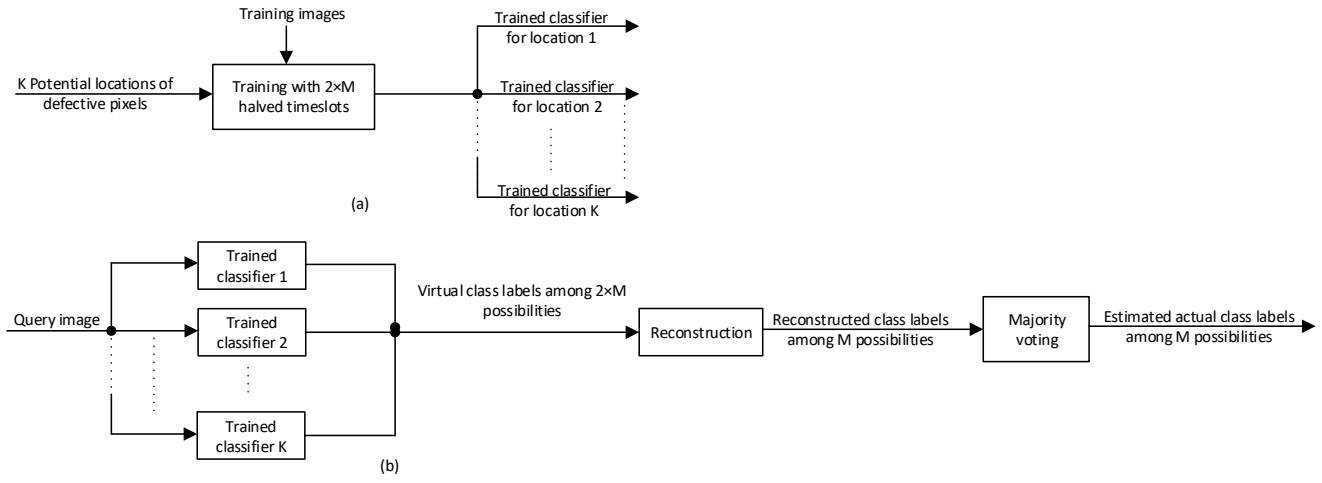


Fig 1.2. Second Stage of the Proposed System

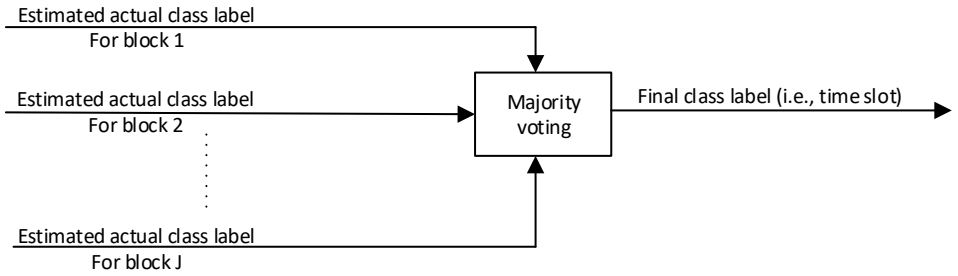


Fig 1.3. Third Stage of the Proposed System

Fig 1. High-Level of the Proposed System

The further description of the proposed system is detailed below in subsections 3.1 to 3.5.

### 3.1. Feature Extraction Process using Pixel Neighborhood and Local Variation (LV) features

Our first aim is to extract the number of pixel locations used as a reliable features for acquisition time estimation. To this end, the behaviour of pixels over time is analyzed to identify the reasonable candidates of the defective pixels. Here, the detection of potential defective pixels based on local neighbourhood is adopted because colour interpolation involves neighbouring pixels and hence the effect of a pixel defect could be spread to its neighbours. The rationale behind estimating potential defective pixels using neighbourhood is that defective pixels exhibit specific and constant behaviour through images over time, unlike other ordinary pixels. Defective pixels are constant, and they did not depend on any external conditions.

The full resolution image is first divided into non-overlapping image blocks of size $W \times H$. Then, the neighbourhood of each pixel is considered in a window of size $w \times w$. Within a moving window of size $w \times w$, $x_c$ is the centre pixel location value which is under examination. The concatenation of pixel intensities extracted for each color channel (Red, Green and Blue) within the window of size $w \times w$ represent the feature vector for a centre pixel location $x_c$.

Here, the centre pixel and its neighbourhood pixel values play a significant role to get the pixel location classified as a defective pixel for our proposed algorithm. In addition, we propose two attributes as the first order local variation LV1 and second order local variation LV2 for every centre pixel location and each color channel. The local variation features for an image block are computed for the red, green and blue channel pixel values within a $w \times w$ window. This window then moves one pixel at a time over the entire image block.

The statistical features of an image such as local variation of a centre pixel within a $w \times w$ window is computed because local regions of an image exhibit more color variations than usual, and can lead to high interpolation errors that could be interpreted as being caused by a defective pixel. The centre pixel value at location $(i, j)$ is denoted by $x_c$, then the local variation features in a $w \times w$ window is given as:

$$LV1 = abs(x_c\text{- avg}) \quad (1)$$

where

$$avg = \frac{\sum_{i=1}^{w}\sum_{j=1}^{w} x_{i,j} - x_c}{w \times w - 1}$$

$$LV2 = sqrt\left(\frac{\sum_{i=1}^{w}\sum_{j=1}^{w} (x_{i,j} - x_c)^2}{w \times w - 1}\right) \quad (2)$$

### 3.2 First training process of Individual Classifiers in each Image Block

Once the features are extracted at each centre pixel location in a $W \times H$ block, a classifier is trained with respect to each centre pixel location using training sample images. To detect the best candidates of defective pixel locations, a multi-class classifier is trained, and its performance is determined on a validation subset of images. It is worth noting here that each class label corresponds to a specific timeframe. Figure 2 is showing the extraction of R, G and B features with concatenation of local variation measures using a number of training images subset for one centre pixel location.

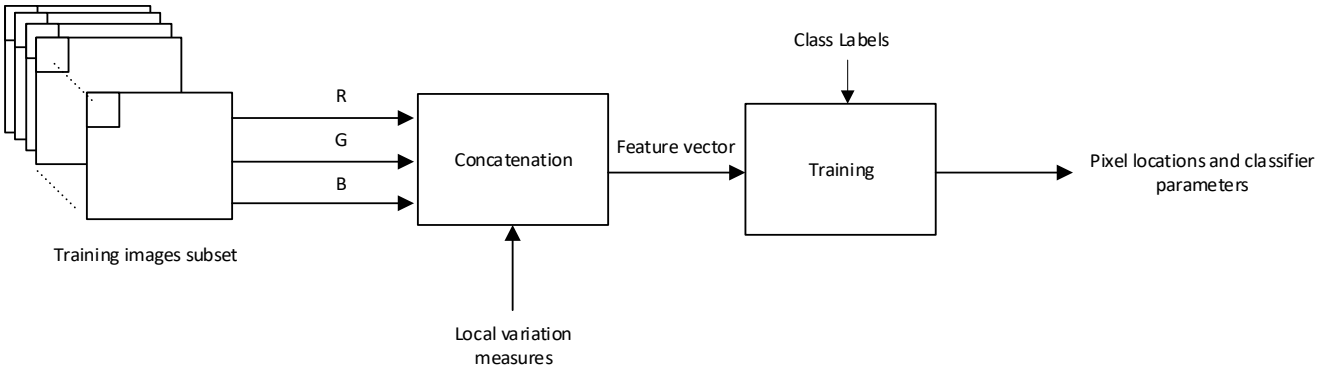


Fig.2. Training of a single classifier corresponding to one fixed centre pixel location for Single Image Block.

### 3.3 Detection of Potential Defective Pixel Locations over Time

In each block of size $W \times H$, all pixel locations are used to train classifiers accordingly and assess their performance on a validation subset. That is, the number of classifiers in a block is almost the same number of pixels in that block with the exception of those pixels at the borders. Once all classifiers are trained, they are validated on validation subset to find potential defective pixel locations. The best $K$ defective pixel locations are selected corresponding to the highest performance obtained. This is to discard the weak classifiers as their contribution to the final system would be insignificant. The process is conducted by sorting the scores of the classifiers in a descending order and taking the top $K$ locations as shown in Figure 3.

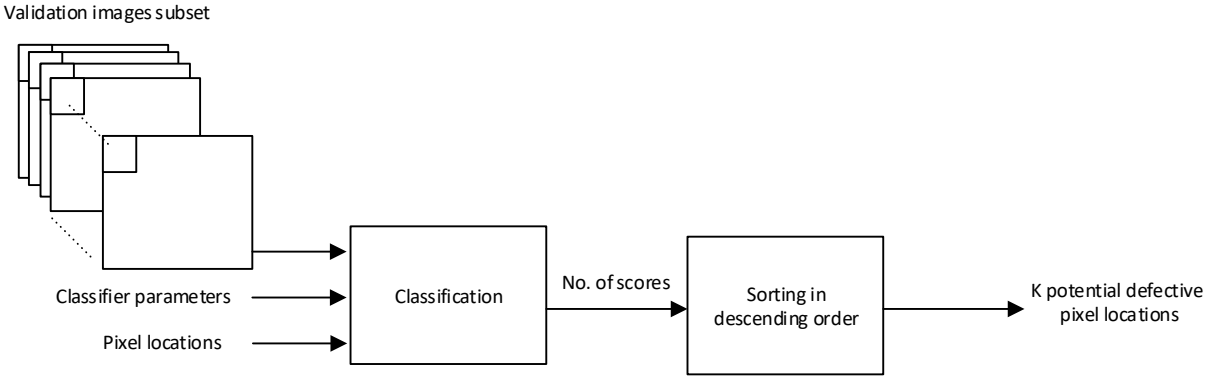


Fig.3. Filtering out the weak classifiers and selection of potential defective pixel locations

### 3.4 Re-Training with Virtual Timeslots and Reconstruction Process

Once the best $K$ defective locations are detected from the previous stage, the corresponding classifiers are re-trained by combining both training and validation subset of images according to the selected $K$ defective pixel locations. Note that this is carried out on virtual sub-classes where each sub-class represents a virtual timeslot by halving the actual timeslots (see Fig. 4). As will be demonstrated in experiments, this proposed idea enhances the accuracy of the system since the classifiers are trained in a more challenging scenario (shorter timeslots and less training samples for each sub-class when compared to actual classes). Each trained classifier corresponding to a specific defective pixel location can predict a virtual timeslot, accordingly.

Given a test image, non-overlapping blocks will be considered accordingly in a similar fashion as in the training stage where each block will have $K$ location-based re-trained classifiers. The location-based decisions in the form of class labels for each image block are first obtained for virtual subclasses. The virtual timeslot is first used to reconstruct the actual class label for each location-based classifier. The representation of actual timeslots in relation to virtual timeslots is shown in Figure 4. The total number of timeslots used for classification is denoted by $M$. Each actual timeslot/class is spanned over a duration $T$.

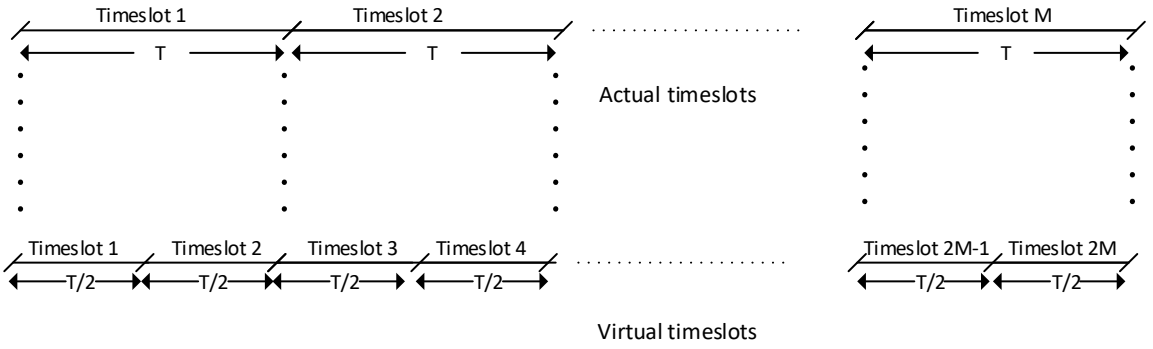


Fig.4. Overview of Actual and Virtual Timeslots

Once the actual class label is reconstructed for each re-trained location-based classifier, the final decision for one image block can be reached through the majority voting method, also referred to as the fusion method in Fig. 5. This method takes the most occurred class label among all $K$ re-trained classifiers' outputs within a given image block.

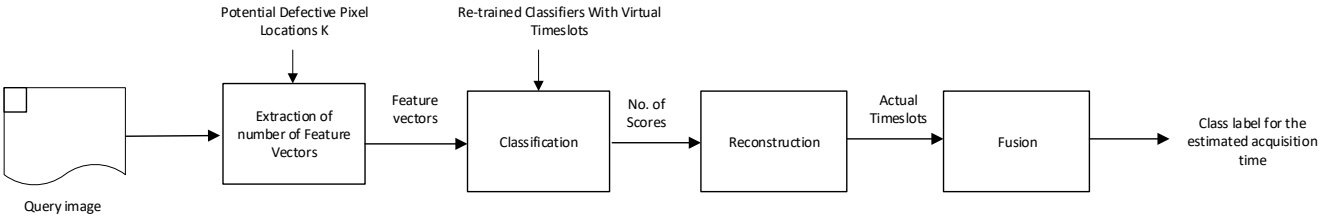


Fig.5. Prediction of Actual Timeslots for a Query Image from Single Image Block $W \times H$

Figure 6 further depicts the process of estimating the acquisition timeslot for a single Image block $W \times H$ using $K$ re-trained location-based classifiers.

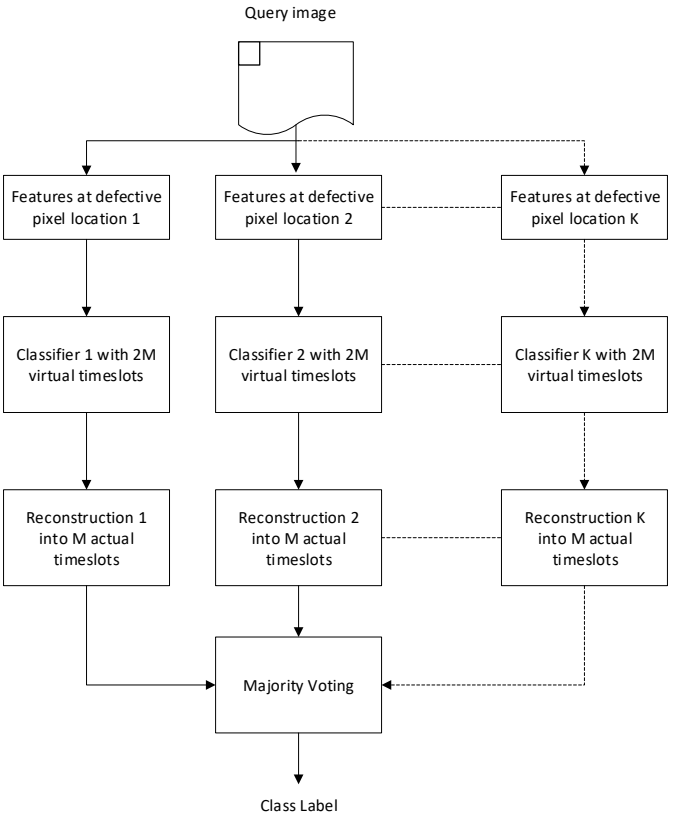


Fig.6. Acquisition Time Estimation of Query Image for Single Image Block $W \times H$

### 3.5 Combination of Blocks for boosting Performance

The last stage of the system combines the predicted class labels on a number of image blocks to boost the performance of the system as will be demonstrated later. In fact, the predicted timeslot by the system is nothing but the combination of scores obtained on non-overlapping blocks through a second majority voting approach. It is believed that potential defective pixels might occur in different spatial areas and hence including them could contribute efficiently to the picture dating process.

## 4. Experimental Results and Analysis

The proposed system is assessed through a number of experiments with different types of classifiers in the first experiment. Mainly three multi-class classifiers were used to evaluate the system: k-Nearest Neighbor (KNN), Error-correcting output codes (ECOC) with by default SVM binary learner (SVM) and the Naïve Bayes classifier. In all experiments, accuracy is measured by the proportion of images that have been correctly assigned to the right acquisition timeslot to the total number of test images.

### 4.1 Image dataset

To gauge the effectiveness of acquisition time estimation on digital pictures for our proposed approach, the database of natural images called Northumbria Temporal Image Forensics (NTIF) is considered (Ahmed et al., 2020). The series of images in the NTIF database have been taken at different times with regular acquisition timeslots spanned over for 94 weeks using ten digital camera devices. A total of 41,684 images were captured from 10 digital cameras with different models and brands. The number of images were captured on a weekly and bi-weekly basis for a number of timeslots for each camera, which makes the NTIF dataset unique and beneficial for this particular problem (Ahmed et al., 2020). Lawgaly and Khelifi (2016), Al-Ani and Khelifi

(2016) and Lawgaly et al. (2014) used this unique dataset of images in their studies for source camera identification (SCI). Also, the NTIF dataset has been used in a study, which is based on a comparative analysis of deep learning for SCI (Ahmed et al., 2019). The NTIF dataset is publically accessible at the following URL: https://github.com/Northumbria-CIS/Northumbria-Temporal-Image-Forensics-NTIF-Database

In our experiments, all digital cameras in the NTIF database are tested. Table 1 shows the image resolutions and the type of sensor for each of the ten cameras used. From the NTIF database, the first 40 weeks were selected for 5 actual classes as shown in Table 2 where 8 weeks were grouped as one class. The reason for choosing 8 weeks in one class is because the occurrence of defective pixels appear in a period of two months, approximately (Fridrich and Goljan, 2011). The 5 actual classes represent a time period that ranges from 21st October 2014 to 24th September 2015 for each camera. For each actual class, the number of training images was 240, whereas 80 validation images were used and 80 test images were considered for every digital camera. As explained earlier, the validation images will be included at the re-training stage once the potential defective pixels are detected. Therefore, the re-training dataset has a total of 1600 images.

Table 1. Characteristics of Ten Digital Cameras

| Camera Model | Resolution | Type of Sensor |
|---|---|---|
| Canon IXUS115HS-1 | 4000 × 3000 | 1/2.3", CMOS |
| Fujifilm S2950-1 | 4288 × 3216 | 1/2.3", CCD |
| Nikon Coolpix L330-1 | 5152 × 3864 | 1/2.3", CCD |
| Panasonic DMC TZ20-1 | 4320 × 3240 | 1/2.33", CMOS |
| Samsung p1120-1 | 4320 × 3240 | 1/2.33", CCD |
| Canon IXUS115HS-2 | 4000 × 3000 | 1/2.3", CMOS |
| Fujifilm S2950-2 | 4288 × 3216 | 1/2.3", CCD |
| Nikon Coolpix L330-2 | 5152 × 3864 | 1/2.3", CCD |
| Panasonic DMC TZ20-2 | 4320 × 3240 | 1/2.33", CMOS |
| Samsung p1120-2 | 4320 × 3240 | 1/2.33", CCD |

Table 2. Summary of the Dataset used in Experimental Study for 5 Actual Classes

| No. of Classes | Date of Images | No. of Training Images | No. of Validation Images | No. of Testing Images |
|---|---|---|---|---|
| Class-1 (Week1-Week8) | 21-10-2014 to 14-12-2014 | 240 | 80 | 80 |
| Class-2 (Week9-Week16) | 22-12-2014 to 13-02-2015 | 240 | 80 | 80 |
| Class-3 (Week17-Week24) | 23-02-2015 to 22-04-2015 | 240 | 80 | 80 |
| Class-4 (Week25-Week 32) | 07-05-2015 to 01-07-2015 | 240 | 80 | 80 |
| Class-5 (Week33-Week40) | 09-07-2015 to 24-09-2015 | 240 | 80 | 80 |
| **Total** | **40 Timeslots** | **1200** | **400** | **400** |

### 4.2 Single block estimation with different classifiers

In the first set of experiments, only pixel neighborhood features (i.e., the neighbourhood of the centre pixel) are considered using a single image block of size $200 \times 200$ where the window size for constructing the feature vector is $3 \times 3$. Here, the idea of virtual sub-classes is not considered since the purpose of this experiment is to assess the performance of different classifiers in order to tune the system. For every centre pixel location, 27 pixel neighborhood features (nine from each colour channel) are extracted to be used in the training stage. For each location in the block, except the ones at the borders, a classifier is trained and the trained models are validated on the 400 validation images to identify potential defective pixel locations. From the block pixel locations, the best 100 potential candidates of defective pixel locations are selected. The system is then re-trained with combined training and validation images using the selected 100 defective pixel locations. The 100 re-trained classifiers were then selected to predict the acquisition timeslot of test images and their scores are combined through majority voting. Here, the estimation of the acquisition time of 400 test images is assessed through three different multiclass classifiers namely k-NN, SVM and Naïve Bayes. The optimal parameters for k-NN are used as Euclidean distance and k=1. For SVM, the best optimal parameter is chosen as a Gaussian kernel with value 1.3. The default parameters of Naïve Bayes are used in the experiments as the kernel distribution with all four kernel parameters requiring a massive computation time to process the results. Table 3 shows the performance of picture acquisition prediction for ten digital cameras with the aforementioned classifiers. As can be seen, KNN classifier has shown a significantly better performance in predicting the actual timeslot as compared to the other tested classifiers.

Table 3. Accuracy in % for 5 Actual Classes using Pixel Neighborhood Features

| | Pixel Neighborhood Features | | |
|---|---|---|---|
| **Digital Cameras** | **KNN** | **SVM** | **Naïve Bayes** |
| **Canon IXUS115HS-1** | 43.75 | 43.25 | 31.75 |
| **Fujifilm S2950-1** | 39.25 | 39.5 | 28.5 |
| **Nikon Coolpix L330-1** | 43.25 | 38.75 | 26.5 |
| **Panasonic DMC TZ20-1** | 49.25 | 47.75 | 29.25 |
| **Samsung p1120-1** | 45.5 | 41 | 27.5 |
| **Canon IXUS115HS-2** | 48 | 46 | 30.5 |
| **Fujifilm S2950-2** | 45.5 | 40.25 | 31.25 |
| **Nikon Coolpix L330-2** | 45.75 | 40 | 29.25 |
| **Panasonic DMC TZ20-2** | 46.75 | 41.25 | 27.75 |
| **Samsung p1120-2** | 48 | 46.75 | 31.75 |

#### 4.2.1 Contribution of Local Variation (LV) features

In this experiment, the contribution of the proposed local variation features is highlighted. Similar to the previous experiment, the training and retraining processes are repeated but this time the proposed local variation features are included for all colour channels (i.e., 6 LV features as described by (1) and (2)). In Table 4, the performance of the classifiers for picture acquisition timeslot prediction on 400 test images including the local variation features are shown for ten digital cameras.

Table 4. Accuracy in % for 5 Actual Classes using Proposed Local Variation Features

| Digital Cameras | KNN | | SVM | | Naïve Bayes | |
|---|---|---|---|---|---|---|
| | Pixel Neighborhood Features | Pixel Neighborhood and LV Features | Pixel Neighborhood Features | Pixel Neighborhood and LV Features | Pixel Neighborhood Features | Pixel Neighborhood and LV Features |
| **Canon IXUS115HS-1** | 43.75 | **47** | 43.25 | **45.75** | 31.75 | **32.5** |
| **Fujifilm S2950-1** | 39.25 | **40** | 39.5 | **41.75** | 28.5 | **30.25** |
| **Nikon Coolpix L330-1** | 43.25 | **44.25** | 38.75 | **40.75** | 26.5 | **29.5** |
| **Panasonic DMC TZ20-1** | 49.25 | **49.75** | 47.75 | **49** | 29.25 | **29.75** |
| **Samsung p1120-1** | 45.5 | **46.5** | 41 | **42.5** | 27.5 | **29.75** |
| **Canon IXUS115HS-2** | 48 | **50.25** | 46 | **47.75** | 30.5 | **32.25** |
| **Fujifilm S2950-2** | 45.5 | **46.5** | 40.25 | **41.25** | 31.25 | **31.5** |
| **Nikon Coolpix L330-2** | 45.75 | **46** | 40 | **43** | 29.25 | **31** |
| **Panasonic DMC TZ20-2** | 46.75 | **48.5** | 41.25 | **43.5** | 27.75 | **29.25** |
| **Samsung p1120-2** | 48 | **49.5** | 46.75 | **47.75** | 31.75 | **32.5** |

The results showed that the combination of pixel neighborhood and LV features has enhanced the performance of the system for all the tested digital cameras and classifiers. Similar to the previous experiment, the KNN classifier is clearly superior over other classifiers. As the contribution of local variation features enhanced the performance, therefore the other experiments will be conducted using pixel neighborhood and local variation features.

### 4.3 Contribution of virtual subclasses

In this experiment, the only difference from the previous experiment is the introduction of the concept of virtual sub-classes. In this experiment we also use a single block of size $200 \times 200$ from a test image to predict its acquisition timeslot. As part of the proposed system and as explained in section 3.4, each actual class is sub-divided into two virtual sub-classes corresponding to halved timeslots of actual classes as shown in Figure 7. That is, for the scenario of 5 actual classes, 10 virtual subclasses are now used to re-train the system once the potential defective pixels are determined. Therefore, the re-training dataset has a total of 1600 images for the 10 virtual subclasses with 160 images per subclass whereas the testing dataset comprises of a total of 400 images where each subclass contains 40 images. The feature extraction process is the same as discussed earlier.

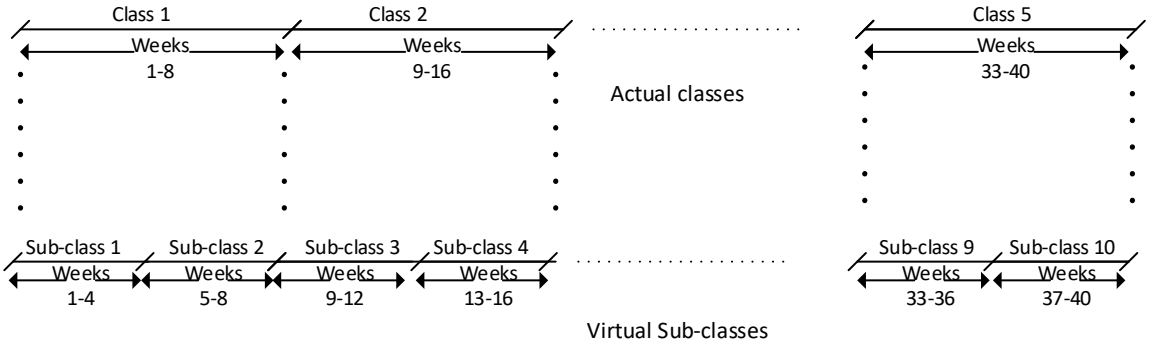


Fig.7. Construction of 10 virtual sub-classes from 5 actual classes

The previous types of classifiers are used again here for the aforementioned 10 digital cameras. As depicted in Table 5, the results show that the concept of re-training with 10 virtual subclasses (i.e., halved timeslots) prior to reconstruction into the 5 actual classes significantly enhanced the performance of the system when compared with the process of directly re-training with 5 actual classes. Furthermore, the results validate our observation on the KNN classifier which again has shown a significantly better performance in predicting the actual timeslot as compared to the other tested classifiers. Consequently, the KNN classifier is adopted in the rest of the paper.

Table 5. Accuracy in % with Reconstruction of 10 Virtual Subclasses into 5 Actual Classes using Single Image Block

| Digital Cameras | KNN | | SVM | | Naïve Bayes | |
|---|---|---|---|---|---|---|
| | 5 Actual Classes | Reconstruction of 10 virtual subclasses into 5 actual classes | 5 Actual Classes | Reconstruction of 10 virtual subclasses into 5 actual classes | 5 Actual Classes | Reconstruction of 10 virtual subclasses into 5 actual classes |
| **Canon IXUS115HS-1** | 47 | **64.75** | 45.75 | **49.25** | 32.5 | **35.25** |
| **Fujifilm S2950-1** | 40 | **56.5** | 41.75 | **44.75** | 30.25 | **31.25** |
| **Nikon Coolpix L330-1** | 44.25 | **57** | 40.75 | **42.75** | 29.5 | **31.25** |
| **Panasonic DMC TZ20-1** | 49.75 | **64.75** | 49 | **54.75** | 29.75 | **30** |
| **Samsung p1120-1** | 46.5 | **62** | 42.5 | **52** | 27.5 | **30.25** |
| **Canon IXUS115HS-2** | 50.25 | **65.75** | 47.75 | **52.25** | 32.25 | **37.25** |
| **Fujifilm S2950-2** | 46.5 | **59** | 41.25 | **44** | 31.5 | **32.5** |
| **Nikon Coolpix L330-2** | 46 | **62.75** | 43 | **45.75** | 31 | **32.75** |
| **Panasonic DMC TZ20-2** | 48.5 | **61.5** | 43.5 | **46** | 29.25 | **30.25** |
| **Samsung p1120-2** | 49.5 | **61.5** | 47.75 | **55** | 32.5 | **33.75** |

### 4.4 Contribution of multi-block score fusion

In this experiment, the contribution of multiple non-overlapping image blocks is combined through majority voting and this is assessed, accordingly using the same dataset. Up to 50 non-overlapping image blocks have been randomly chosen from each image. Results are illustrated in Fig. 8 for the 10 test digital cameras. As can be seen, the performance of the system significantly jumps against the increasing number of combined blocks before it stabilises at around 45 blocks.

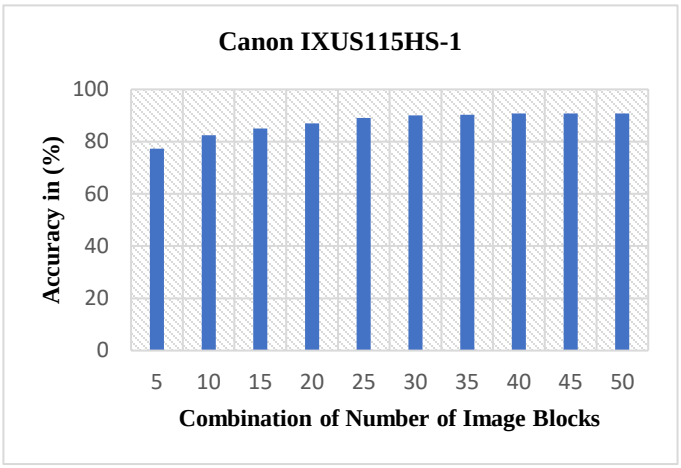


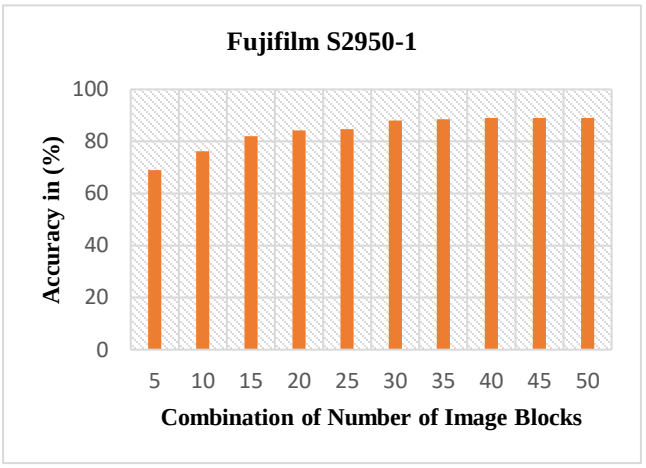


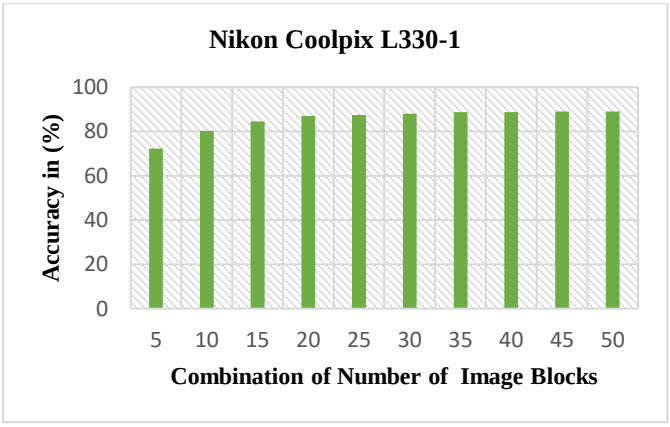


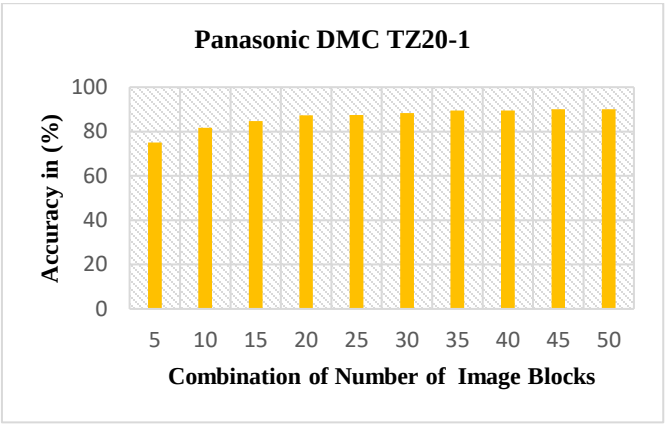


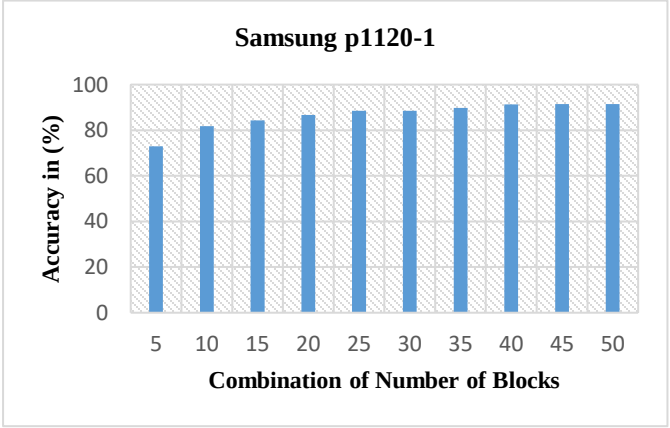


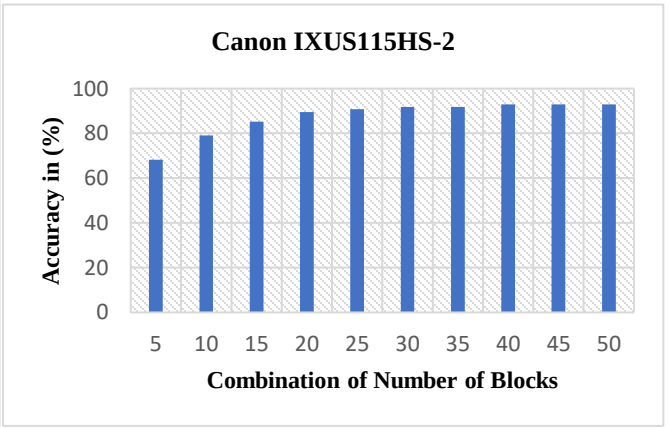

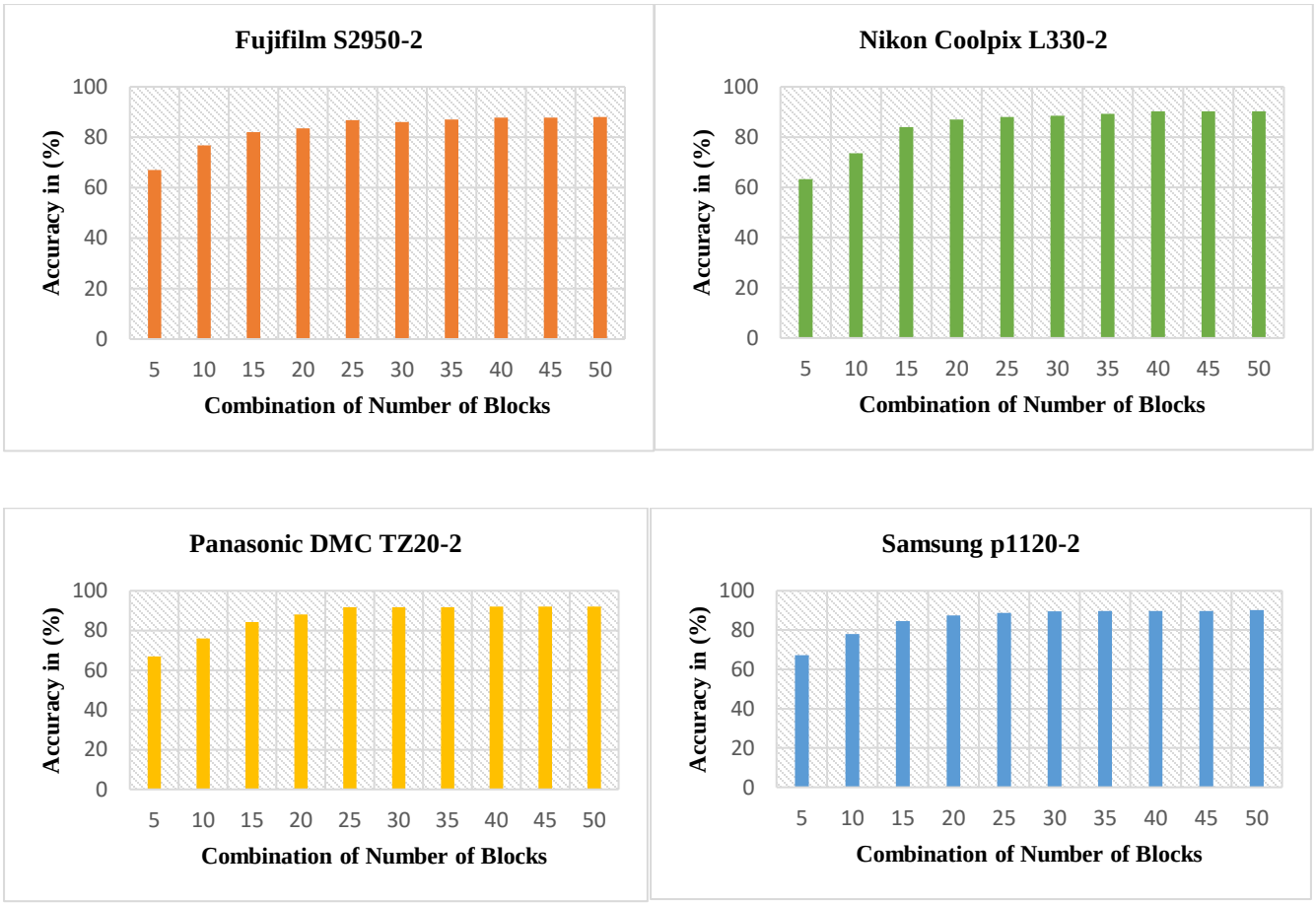


Fig. 8. Accuracy in % on 400 Test Images using the Combination of Blocks (up to 50 blocks) of size $200 \times 200$ for different Digital Cameras

In this experiment, it has been found that the combination of 45 image blocks through majority voting is the optimal parameter to reach the highest accuracy while giving a good tradeoff between performance and computational complexity. Table 6 depicts the accuracy of the system when 45 non-overlapping image blocks were combined as compared to a single block performance for all 10 digital cameras. It can be seen that the proposed system improves considerably with an accuracy varying from 88 to 93 %.

Table 6. Accuracy in % for 10 Digital Cameras using the Combination of 45 Blocks with KNN classifier

| Digital Cameras | Accuracy | |
|---|---|---|
| | Single Block | 45 Multi-Blocks |
| Canon IXUS115HS-1 | 64.75 | **90.75** |
| Fujifilm S2950-1 | 56.5 | **89** |
| Nikon Coolpix L330-1 | 57 | **89** |
| Panasonic DMC TZ20-1 | 64.75 | **90** |
| Samsung p1120-1 | 62 | **91.5** |
| Canon IXUS115HS-2 | 65.75 | **93** |
| Fujifilm S2950-2 | 59 | **88** |
| Nikon Coolpix L330-2 | 62.75 | **90.25** |
| Panasonic DMC TZ20-2 | 61.5 | **92** |
| Samsung p1120-2 | 61.5 | **90.25** |

### 4.5 Comparison with a competing system

In this section, the proposed system is compared with an existing state-of-the-art system, namely Individual Image Placement (IIP) within an ordered cluster set (Mao et al., 2009). For fair comparison, the same number of classes (timeslots) and number of training and test images have been used. Results are depicted in Table 7. The proposed system provides the best performance when compared with the competing technique. The proposed system appears significant more powerful in dealing with the problem of predicting image acquisition timeslot and the results obtained are very promising. In forensic investigations, it is believed that these results can provide the opportunities to the analysts to link different events of crime scenes and to determine reliably the timeframes in which evidential images were captured.

Table 7. Performance of state-of-the-art system and proposed system in % for 10 Digital Cameras

| Digital Cameras | Accuracy | |
|---|---|---|
| | State-of-the-art System | Proposed system |
| Canon IXUS115HS-1 | 46.25 | **90.75** |
| Fujifilm S2950-1 | 41 | **89** |
| Nikon Coolpix L330-1 | 44.75 | **89** |
| Panasonic DMC TZ20-1 | 49 | **90** |
| Samsung p1120-1 | 44 | **91.5** |
| Canon IXUS115HS-2 | 44.75 | **93** |
| Fujifilm S2950-2 | 40.75 | **88** |
| Nikon Coolpix L330-2 | 44.25 | **90.25** |
| Panasonic DMC TZ20-2 | 45 | **92** |
| Samsung p1120-2 | 42.25 | **90.25** |

### 4.6 Computational complexity

In this section, the computation complexity for both techniques is discussed. It is worth that all experiments have been conducted using Matlab (Windows version) on a machine (or work station) HP with 64 GB RAM and 3.00 GHz processor. The computation time for the training and testing stage for each of the techniques is listed in Table 8. For five classes, it is worth noting that that the most time consuming part of the competing technique Mao et al. (2009) resides in the PRNU estimation using all training images, each with a full size of $3240 \times 4320$ . In fact, this process takes 70 seconds approximately per image. For our proposed training stage, the computation time for a single block $200 \times 200$ is 40 minutes using 5 classes. With typical 45 block processing, the computation time at the training stage is around 30 hours for the same digital camera as used with the competing technique. However, although the training stage appears highly time consuming in both methods, this can be conducted offline during the forensic investigation. Once the classifiers are trained, the decision can be reached in a much faster fashion when compared to the training stage.

As illustrated in Table 8, the computation time with the method in (Mao et al., 2009) at the testing stage is slightly faster than our proposed system because it only involves the extraction of a noise residual for one test image (around 70 seconds) while the correlation with the estimated PRNUs from 5 classes is much faster (around 1 second per comparison).

Table 8: The computation time for the training and testing system and Mao et al. (2009) system

| Technique | Training | Testing |
|---|---|---|
| Proposed Technique | 30 Hours | 80 secs |
| Mao et al. (2009) technique | 31 Hours | 75 secs |

## 5. Conclusion

In this paper, several contributions have been made for estimating the acquisition time of digital pictures. The idea uses a combination of an effective defective pixel detection and a machine learning approach to estimate the age of digital pictures. The local variation features were proposed that efficiently detect potential defective pixels for picture dating. Virtual timeslots were introduced prior to the reconstruction step into actual classes. Once the actual class label is reconstructed for each defective pixel location-based classifier, the final decision for a single image block is reached through the majority voting method. To further enhance the performance, a multi-block based machine learning model is used to combine the predicted scores from multiples blocks in a second majority voting operation. Extensive experiments have been performed to evaluate the performance of the proposed system from three different multi-class classifiers for ten digital cameras. The experimental results show that KNN is the best to classify the picture acquisition timeslot prediction using defective pixels. Our results showed very good performance with an estimated accuracy between 88% and 93% when compared with a related state-of-the-art system.

**Acknowledgement**

This work was partially supported by NPRP grant # NPRP12S-0312-190332 from the Qatar National Research Fund (a member of the Qatar Foundation). The statements made herein are solely the responsibility of the authors.

***REFERENCES***


AHMED, F., KHELIFI, F., LAWGALV, A. & BOURIDANE, A. Comparative Analysis of a Deep Convolutional Neural Network for Source Camera Identification. 2019 IEEE 12th International Conference on Global Security, Safety and Sustainability (ICGS3), 2019. IEEE, 1-6.

AHMED, F., KHELIFI, F., LAWGALY, A. & BOURIDANE, A. The 'Northumbria Temporal Image Forensics' Database: Description and Analysis. 2020 7th International Conference on Control, Decision and Information Technologies (CoDIT), 2020. IEEE, 982-987.

AL-ANI, M. & KHELIFI, F. 2016. On the SPN estimation in image forensics: a systematic empirical evaluation. *IEEE Transactions on Information Forensics and Security,* 12**,** 1067-1081.

AL-ANI, M., KHELIFI, F., LAWGALY, A. & BOURIDANE, A. A novel image filtering approach for sensor fingerprint estimation in source camera identification. 2015 12th IEEE International Conference on Advanced Video and Signal Based Surveillance (AVSS), 2015. IEEE, 1-5.

AQUILINA, J. M., CASEY, E., MALIN, C. H. & ROSE, C. W. 2008. *Malware forensics*, Elsevier.

BERNACKI, J. 2020. A survey on digital camera identification methods. *Forensic Science International: Digital Investigation,* 34**,** 300983.

CASEY, E. 2009. *Handbook of digital forensics and investigation,* Academic Press.

CASEY, E. 2020. Standardization of forming and expressing preliminary evaluative opinions on digital evidence. *Forensic Science International: Digital Investigation,* 32**,** 200888.

CASEY, E., KATZ, G. & LEWTHWAITE, J. 2013. Honing digital forensic processes. *Digital Investigation,* 10**,** 138-147.

CHAPMAN, G. H., KOREN, I., KOREN, Z., DUDAS, J. & JUNG, C. On-line identification of faults in fault-tolerant imagers. 20th IEEE International Symposium on Defect and Fault Tolerance in VLSI Systems (DFT'05), 2005. IEEE, 149-157.

CHAPMAN, G. H., LEUNG, J., NAMBURETE, A., KOREN, I. & KOREN, Z. Predicting pixel defect rates based on image sensor parameters. 2011 IEEE International Symposium on Defect and Fault Tolerance in VLSI and Nanotechnology Systems, 2011. IEEE, 408-416.

CHAPMAN, G. H., LEUNG, J., THOMAS, R., NAMBURETE, A., KOREN, Z. & KOREN, I. Projecting the rate of in-field pixel defects based on pixel size, sensor area, and ISO. Sensors, Cameras, and Systems for Industrial and Scientific Applications XIII, 2012. International Society for Optics and Photonics, 82980E.

CHAPMAN, G. H., THOMAS, R., KOREN, I. & KOREN, Z. 2017. Hot Pixel Behavior as Pixel Size Reduces to 1 micron. *Electronic Imaging,* 2017**,** 39-45.

CHAPMAN, G. H., THOMAS, R., KOREN, Z. & KOREN, I. Empirical formula for rates of hot pixel defects based on pixel size, sensor area, and ISO. Sensors, Cameras, and Systems for Industrial and Scientific Applications XIV, 2013. International Society for Optics and Photonics, 86590C.

CHAPMAN, G. H., THOMAS, R., MENESES, K. J., KOREN, I. & KOREN, Z. 2019. Image degradation from hot pixel defects with pixel size shrinkage. *Electronic Imaging,* 2019**,** 359-1-359-7.

CHAPMAN, G. H., THOMAS, R., MENESES, K. J., PURBAKHT, P., KOREN, I. & KOREN, Z. 2018. Exploring Hot Pixel Characteristics for 7 to 1.3 micron Pixels. *Electronic Imaging,* 2018**,** 401-1-401-6.

DONG, S., SUN, X., XIE, S. & WANG, M. 2019. Automatic defect identification technology of digital image of pipeline weld. *Natural Gas Industry B,* 6**,** 399-403.

DUDAS, J., WU, L. M., JUNG, C., CHAPMAN, G. H., KOREN, Z. & KOREN, I. Identification of in-field defect development in digital image sensors. Digital Photography III, 2007. International Society for Optics and Photonics, 65020Y.

EL-YAMANY, N. 2017. Robust Defect Pixel Detection and Correction for Bayer Imaging Systems. *Electronic Imaging,* 2017**,** 46-51.

FERNANDO, B., MUSELET, D., KHAN, R. & TUYTELAARS, T. Color features for dating historical color images. 2014 IEEE International Conference on Image Processing (ICIP), 2014. IEEE, 2589-2593.

FORCINA, A. & CARBONE, P. 2020. Modelling dark current and hot pixels in imaging sensors. *Statistical Modelling,* 20**,** 30-41.

FRIDRICH, J. & GOLJAN, M. Determining approximate age of digital images using sensor defects. Media Watermarking, Security, and Forensics III, 2011. International Society for Optics and Photonics, 788006.

GINOSAR, S., RAKELLY, K., SACHS, S., YIN, B. & EFROS, A. A. A century of portraits: A visual historical record of american high school yearbooks. Proceedings of the IEEE International Conference on Computer Vision Workshops, 2015. 1-7.

GUPTA, B. & TIWARI, M. 2018. Improving source camera identification performance using DCT based image frequency components dependent sensor pattern noise extraction method. *Digital Investigation,* 24**,** 121-127.

HE, S., SAMARA, P., BURGERS, J. & SCHOMAKER, L. 2016. Image-based historical manuscript dating using contour and stroke fragments. *Pattern Recognition,* 58**,** 159-171.

IGOE, D. P., PARISI, A. V., AMAR, A. & RUMMENIE, K. J. 2018. Median filters as a tool to determine dark noise thresholds in high resolution smartphone image sensors for scientific imaging. *Review of Scientific Instruments,* 89**,** 015003.

JAE LEE, Y., EFROS, A. A. & HEBERT, M. Style-aware mid-level representation for discovering visual connections in space and time. Proceedings of the IEEE international conference on computer vision, 2013. 1857-1864.

KAKAR, P. & SUDHA, N. 2012. Verifying temporal data in geotagged images via sun azimuth estimation. *IEEE Transactions on Information Forensics and Security,* 7**,** 1029-1039.

KAUBA, C. & UHL, A. Prnu-based image alignment for defective pixel detection. 2016 IEEE 8th International Conference on Biometrics Theory, Applications and Systems (BTAS), 2016. IEEE, 1-7.

LAWGALY, A. & KHELIFI, F. 2016. Sensor pattern noise estimation based on improved locally adaptive DCT filtering and weighted averaging for source camera identification and verification. *IEEE Transactions on Information Forensics and Security,* 12**,** 392-404.

LAWGALY, A., KHELIFI, F. & BOURIDANE, A. Weighted averaging-based sensor pattern noise estimation for source camera identification. 2014 IEEE International Conference on Image Processing (ICIP), 2014. IEEE, 5357-5361.

LEE, S., MAISONNEUVE, N., CRANDALL, D., EFROS, A. A. & SIVIC, J. Linking past to present: Discovering style in two centuries of architecture. IEEE International Conference on Computational Photography, 2015.

LEUNG, J., CHAPMAN, G. H., KOREN, I. & KOREN, Z. Automatic detection of in-field defect growth in image sensors. 2008 IEEE International Symposium on Defect and Fault Tolerance of VLSI Systems, 2008a. IEEE, 305-313.

LEUNG, J., CHAPMAN, G. H., KOREN, Z. & KOREN, I. Statistical identification and analysis of defect development in digital imagers. Digital Photography V, 2009. International Society for Optics and Photonics, 72500W.

LEUNG, J., DUDAS, J., CHAPMAN, G. H., KOREN, I. & KOREN, Z. Quantitative analysis of in-field defects in image sensor arrays. 22nd IEEE International Symposium on Defect and Fault-Tolerance in VLSI Systems (DFT 2007), 2007. IEEE, 526-534.

LEUNG, J., DUDAS, J., CHAPMAN, G. H., KOREN, Z. & KOREN, I. Characterization of pixel defect development during digital imager lifetime. Sensors, Cameras, and Systems for Industrial/Scientific Applications IX, 2008b. International Society for Optics and Photonics, 68160A.

LI, X., XU, W., WANG, S. & QU, X. Are you lying: Validating the time-location of outdoor images. International Conference on Applied Cryptography and Network Security, 2017. Springer, 103-123.

LUKÁŠ, J., FRIDRICH, J. & GOLJAN, M. 2006. Digital camera identification from sensor pattern noise. *IEEE Transactions on Information Forensics and Security,* 1**,** 205-214.

MAO, J., BULAN, O., SHARMA, G. & DATTA, S. Device temporal forensics: An information theoretic approach. 2009 16th IEEE International Conference on Image Processing (ICIP), 2009. IEEE, 1501-1504.

MARTIN, P., DOUCET, A. & JURIE, F. Dating color images with ordinal classification. Proceedings of International Conference on Multimedia Retrieval, 2014. ACM, 447.

MÜLLER, E., SPRINGSTEIN, M. & EWERTH, R. "When was this picture taken?"–Image date estimation in the wild. European Conference on Information Retrieval, 2017. Springer, 619-625.

PADILHA, R., ANDALÓ, F. A., LAVI, B., PEREIRA, L. A. & ROCHA, A. 2021a. Temporally sorting images from real-world events. *Pattern Recognition Letters,* 147**,** 212-219.

PADILHA, R., SALEM, T., WORKMAN, S., ANDALÓ, F. A., ROCHA, A. & JACOBS, N. 2021b. Content-Based Detection of Temporal Metadata Manipulation. *arXiv preprint arXiv:2103.04736*.

PALERMO, F., HAYS, J. & EFROS, A. A. Dating historical color images. European Conference on Computer Vision, 2012. Springer, 499-512.

RYSER, E., SPICHIGER, H. & CASEY, E. 2020. Structured decision making in investigations involving digital and multimedia evidence. *Forensic Science International: Digital Investigation,* 34**,** 301015.

SALEM, T., WORKMAN, S., ZHAI, M. & JACOBS, N. Analyzing human appearance as a cue for dating images. 2016 IEEE Winter Conference on Applications of Computer Vision (WACV), 2016. IEEE, 1-8.

TCHENDJOU, G. T. & SIMEU, E. 2020. Detection, Location and Concealment of Defective Pixels in Image Sensors. *IEEE Transactions on Emerging Topics in Computing*.

THEUWISSEN, A. J. 2007. Influence of terrestrial cosmic rays on the reliability of CCD image sensors—Part 1: Experiments at room temperature. *IEEE Transactions on Electron Devices,* 54**,** 3260-3266.

VITTAYAKORN, S., BERG, A. C. & BERG, T. L. When was that made? 2017 IEEE Winter Conference on Applications of Computer Vision (WACV), 2017. IEEE, 715-724.

WANG, W., ZHU, T., FU, Y.-T. & DONG, F. A new blind-pixel detection method for 384× 288 long-wave infrared focal plane arrays images. 9th International Symposium on Advanced Optical Manufacturing and Testing Technologies: Optoelectronic Materials and Devices for Sensing and Imaging, 2019. International Society for Optics and Photonics, 108431T.